# Analysis of Porphyrines as Catalysts for Electrochemical Reduction of O_2 and Oxidation of H_2O

Jakub D. Baran,* Henrik Grönbeck, and Anders Hellman*

Competence Centre for Catalysis and Department of Applied Physics, Chalmers University of Technology, SE-412 96, Göteborg, Sweden

S *Supporting Information*

ABSTRACT: Bioinspired structures are promising as improved catalysts for various redox reactions. One example is metal hangman-porphyrines (MHP), which recently have been suggested for oxygen reduction/evolution reaction (ORR/OER). The unique properties of the MHPs are attributed to both the hangman scaffold and the C_6F_5 side groups. Herein, the OER/ORR over various transition metal MHPs is investigated by density functional theory calculations within an electrochemical framework. A comparison of the reaction landscape for MHP, metal porphyrine (MP) and metaltetrafluorophenyloporphyrines (MTFPP), allow for a disentanglement of the different roles of the hangman motif and the side groups. In agreement with experimental studies, it is found that Fe and Co are the best MHP metal centers to catalyze these reactions. We find that the addition of the three-dimensional moiety in the form of hangman scaffold does not break the apparently universal energy relation between *OH and *OOH intermediates. However, the hangman motif is found to stabilize the oxygen intermediate, whereas addition of C_6F_5 groups reduces the binding energy of all reaction intermediates. Our results indicate that the combination of these two effects allow new design possibilities for macromolecular systems with enhanced catalytic OER/ORR activity.
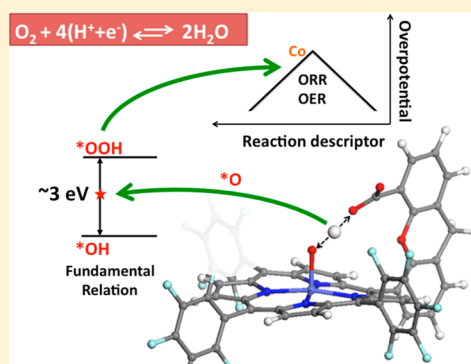
INTRODUCTION

Low temperature fuel cells are attracting considerable interest for production of electricity by direct electrochemical conversion of hydrogen and oxygen into water.[1] In the same fashion, electrolysis of water to hydrogen and oxygen is a key component in a future sustainable society.[2,3] There are, however, severe shortcomings of the present technology, which need to be overcome in order to make these technologies economically viable. One is the substantial overpotential at the oxygen electrodes,[4,5] and another is the high cost of current electrode materials, which normally contain precious metals such as Pt, Ir, and Ru.[6,7] Large efforts have, consequently, been directed toward the development of novel electrode materials for the oxygen reduction (ORR) and oxygen evolution (OER) reactions. In this respect, one important observation is that binding strength between OER/ORR intermediates and electrode material appears to be correlated.[4] In fact, a constant energy separation of around 3.2 eV has been found between *OOH and *OH intermediates for various materials including graphene with M-N_4 centers,[8] metals,[4] and oxide surfaces.[9] From a thermodynamical standpoint (see Discussion below), in case of an ideal catalyst, the energy difference between these two electrochemical steps is expected to be of 2.46 eV. Thus, a minimum overpotential for these materials of ~0.37 eV is introduced that originates from the *OH−*OOH energetic relation alone. The reason for this scaling relation is still under debate, and one component has

been suggested to be the structural properties of current catalyst materials. As compared to highly effective processes in biological respiratory system,[10,11] the current catalyst materials are based on rigid metal or oxide surfaces/particles, which cannot match the flexibility of the active center of the enzymes. Moreover, enzymes possess a secondary coordination sphere that provides noncovalent interactions to the adsorbate and is believed to have considerable impact on the reactivity and selectivity of the reaction intermediates. In fact, the secondary coordination sphere appears to be a necessity in order to overcome energy barriers arising from the triplet ground state of the oxygen.[10] The design of catalyst materials that mimic the secondary coordination sphere interaction to the adsorbate is very difficult task and thus often relegated to the solvation effect.

A particularly interesting route for improved electrode materials is bioinspired catalysts, i.e., synthetic materials based on the unique catalytic efficiency of metalloenzymes that occur naturally, such as Cytochrome P450 and Haem peroxidases. In this respect, phthalocyanines, porphyrins, and their variations have gained considerable attention as promising catalysts for OER/ORR.[10,12−19] The interest originates from their structural similarity with vital biomolecules that appear in the center of common enzymes. The active site in these molecules is
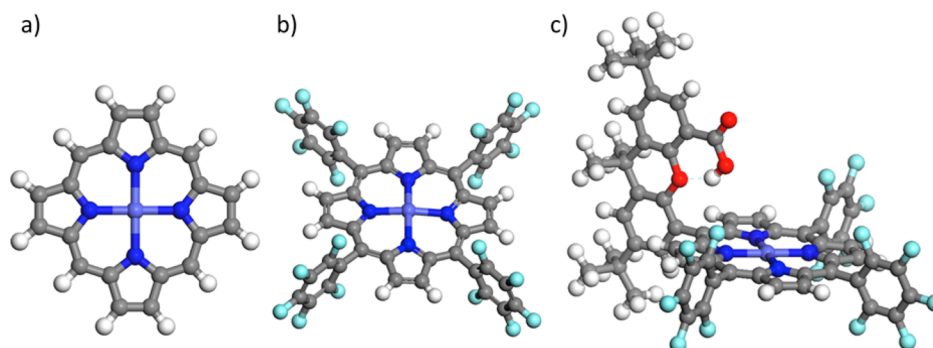
Figure 1. The atomic structure of (a) MP, (b) MTFPP, and (c) MHP. Gray spheres represent C; red, O; dark blue, N; light blue, M; green, F; and white, H, respectively.

generally transition metal (M) coordinated to nitrogen atoms, see Figure 1. A further step in the design of bioinspired catalysts for the OER/ORR is the so-called "hangman" metalloporphyrins (MHPs), which recently have been synthesized and evaluated by Nocera and co-workers; see Figure 1c.[20−24] The MHPs contain a xanthene backbone with a hanging caroboxylic acid group that could serve as a proton supplier and/or acceptor. Interestingly, the MHP has been measured to have a much higher activity for the OER/ORR than the corresponding metalloporphyrines without the hangman motif.[21]

Despite the promising properties of the MHPs, fundamental understanding of the underlying mechanisms for the high performance is presently scarce. Such understanding is required for further design of efficient catalysis with bioinspired molecules as templates.

Herein, density functional theory calculations are used within an electrochemical framework to analyze the OER/ORR reaction over MP, MTFPP, and MHP (see Figure 1) with various transition-metal atoms in the center of porphyrine cores. In particular, the stability of the reaction intermediates *OOH, *O, and *OH is calculated, which allows for evaluation of the thermodynamical OER/ORR overpotentials for these systems. This allows the construction of volcano plots over the reaction activity (here overpotential) vs reaction descriptor, and consequently the identification of the most catalytically active metals for these systems. Moreover, by a thorough comparison between the stability of reaction intermediates between MP, MTFPP, and MHP, we provide an atomistic insight into different roles of the hangman scaffold and the side groups. Although the study presented here is based on thermodynamical consideration, it should account qualitatively also for the reaction kinetics.[4]

COMPUTATIONAL METHODS

The all-electron density functional theory (DFT) calculations with scalar relativistic core treatment are performed by use of the DMol³ program[25−27] with the gradient-corrected exchange-correlation functional BLYP.[28] All calculations are performed spin-unrestricted, and the spin configuration of the ground state is carefully investigated for each system. The one-electron Kohn−Sham orbitals are expanded in a localized numerical basis set. A double numerical basis set is used together with polarization functions (DNP). A real space cutoff of 5 Å is used for the basis functions. The Kohn−Sham equations are solved self-consistently using an integration technique based on weighted overlapping spheres centered at each atom. The direct Coulomb potential is obtained by projection of the charge density onto angular dependent weighting functions also centered at each atom. The Poisson equation is, thereafter, solved by one-dimensional integration. The self-consistent-field (SCF) procedures are performed with a

convergence criterion of 1×10^{-5} Ha on the total energy. Geometry optimizations are performed by the use of the BFGS method,[29] and the structures are considered to be relaxed when the largest element of the gradient is below 1×10^{-3} Ha/Å. No symmetry constraints are imposed during the geometry optimization. The adiabatic ionization potentials (IPs) are calculated as the difference in total energies between the neutral and ionized complexes in the corresponding geometrical ground state.

It has been demonstrated that the electronic configuration of these systems is sensitive to the choice of DFT functional and basis set.[30] Different exchange-correlation (XC) functionals produce different energies and mixing for orbitals with substantial contributions from the M-d states.[30] Some of these properties may not be fully described by any DFT method.[31] For instance, one needs to note that crossover effects can influence the reactivity of these transition metal complexes.[32] However, we applied the above methodology because (i) it gives a very good agreement between calculated and available crystallographic structure of the molecules (see Supporting Information); (ii) trend studies are not very sensitive to systematic errors that occur from the central metal atoms; and (iii) the methodology is able to identify the most efficient catalysts, which is experimentally determined.

To study the OER/ORR, the electrochemical framework developed by Nørskov, Rossmeisl, and co-workers is used.[4,33,34] In the reaction energy landscape, all intermediates are described as single proton transfers, coupled with single electron transfers. In this way, the ORR ($O_2 + 4(H^+ + e^-) \rightarrow 2H_2O$) is split into four electrochemical intermediate steps with the consecutive formation of three reaction intermediates, namely, *OOH, *O, and *OH (* denotes the M-site in the complexes). The enthalpy changes in the formation of the reaction intermediates are calculated as

$$\Delta E_{*OOH}^{ORR} = E_{*OOH}^{DFT} - E_*^{DFT} - E_{O_2}^{DFT} - (H^+ + e^-) \tag{1}$$

$$\Delta E_{*O}^{ORR} = E_{*O}^{DFT} - E_*^{DFT} - \frac{1}{2}E_{O_2}^{DFT} + H_f(H_2O) \tag{2}$$

$$\Delta E_{*OH}^{ORR} = E_{*OH}^{DFT} - E_*^{DFT} - \frac{1}{2}E_{O_2}^{DFT} - (H^+ + e^-) + H_f(H_2O) \tag{3}$$

$$\Delta E_{H_2O}^{ORR} = 2H_f(H_2O) \tag{4}$$

Here, E_{*OOH}^{DFT}, E_{*O}^{DFT}, E_{*OH}^{DFT} is the calculated total energy of the intermediate reaction complexes, whereas E_*^{DFT} is the total energy of the free catalyst molecule. Note that any temperature dependence of the enthalpy of the reaction intermediates is neglected in the calculations. $H_f(H_2O)$ is the experimental formation enthalpy (−2.46 eV) of a single H_2O molecule. The reference energy for O_2 in the gas phase is calculated as

$$E_{O_2(g)} = 4.92 \text{ eV} + 2(E_{H_2O}^{DFT} - E_{H_2}^{DFT})$$

This procedure is chosen because of the well-known difficulties to accurately describe molecular oxygen within DFT.[35] The enthalpies are given with respect to the reversible hydrogen electrode (RHE). At RHE, $(H^+ + e^-)$ equals, by definition, the total energy of $1/2$ H_2 (in the gas phase, under standard condition).[4] The corresponding Gibbs free energies are calculated according to

$$\Delta G = \Delta E + \Delta ZPE - T\Delta S^0 + k_B T \ln a_{H^+} + eU$$

ΔE is given by eq 1–3, and ΔZPE and ΔS^0 are the differences in zero point energy and entropy arising from the reaction, respectively, and are taken from tabulated data.[4] We have verified this approximate correction by performing explicit vibrational calculations of the reaction intermediates of MP with three central metal atoms, i.e., Cr, Co, and Cu, that span whole range of energies that are dealt with in this study. Our calculations reveal that the average $\Delta ZPE - T\Delta S$ corrections to ΔE are 0.04/0.28/0.32 eV for *O/*OH/*OOH species of MP. This is very close to the correction used from the literature, namely, 0.05/0.30/0.35 eV.[4]

$k_B T \ln a_{H^+}$ is the change of free energy owing to the concentration of H^+, k_B is the Boltzmann constant, and T is the temperature. Henceforth, pH ($\ln a_{H^+}$) is set to zero. As OER ($2H_2O \rightarrow O_2 + 4(H^+ + e^-)$) is the reverse of ORR, the Gibbs free energies of the OER are related to ORR intermediates by the reference of -4.92 eV, i.e., $\Delta G_{intermediate}^{OER} = \Delta G_{intermediate}^{ORR} + 4.92$ eV.

The Gibbs free energy differences between OER/ORR intermediates are used to obtain the highest theoretical electrode potential at standard potential for which all the elementary steps are exothermic and downhill in energy.

$$U^{0,ORR} = \{-\max[\Delta G_{*OOH}^{ORR}, \Delta G_{*O}^{ORR} - \Delta G_{*OOH}^{ORR}, \Delta G_{*OH}^{ORR} - \Delta G_{*O}^{ORR}, -4.92 \text{ eV} - \Delta G_{*OH}^{ORR}]\}/e$$

$$U^{0,OER} = \{\max[\Delta G_{*OH}^{OER}, \Delta G_{*O}^{OER} - \Delta G_{*OH}^{OER}, \Delta G_{*OOH}^{OER} - \Delta G_{*O}^{OER}, 4.92 \text{ eV} - \Delta G_{*OOH}^{OER}]\}/e$$

We use calculated $U^{0,ORR}$ and $U^{0,OER}$ to define theoretical thermodynamical OER/ORR overpotential as

$$\eta^{0,ORR} = U^0 - U^{0,ORR}$$

$$\eta^{0,OER} = U^0 - U^{0,OER}$$

where $U^0 = 1.23$ V is the maximum electrode potential allowed by thermodynamics.

In the calculation of OER/ORR overpotentials, the Gibbs free energies of *OOH and *OH are corrected because of the presence of solvation as described in ref 8. This correction accounts for energy contributions that arise from hydrogen bonds between the adsorbate and the adjacent water molecules in the solvent. The additional hydrogen bond energy in liquid has been experimentally estimated to be ~0.15 eV.[8,36] Since *OH and *OOH can participate in the formation of two hydrogen bonds (one donor and one acceptor), a 0.30 eV correction has been used for *OH/*OOH of MPs and MTFPPs. However, the hanging carboxylic group, as will be discussed later, already provides one hydrogen bond to the adsorbate; thus, energies of *OH/*OOH of MHP complexes have been corrected by 0.15 eV. To check this assumption, an explicit solvation model, the PCM, has been used on the CoP, and the results are only affected on the scale of a few hundredth of eV.

RESULTS AND DISCUSSION

Figure 2 shows relation between Gibbs free energy of *OH, *O, and *OOH for various MPs, MTFPPs, and MHPs.

From our results it is clear that there is a universal scaling relation between the ΔG of *OH and *OOH with the separation of ~3.0 ($\pm$0.05) eV, regardless of the central metal atom and modification of the macrocycle. This is in agreement with previous studies of metals, oxides, graphene, and
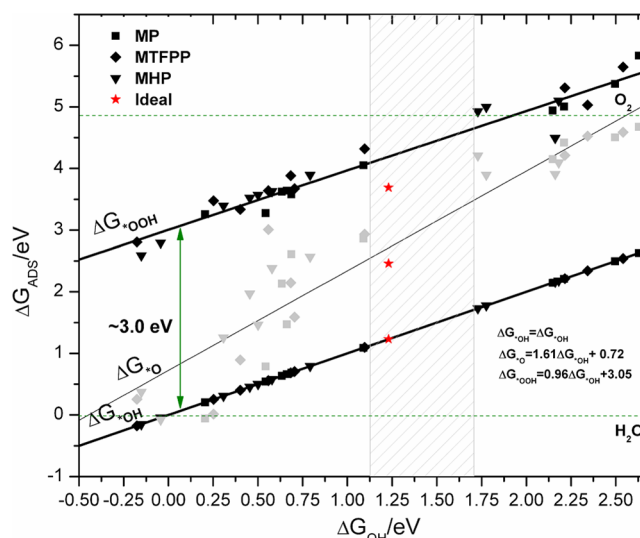
Figure 2. Scaling relation between the Gibbs free energies of adsorption of *OH, *O, and *OOH. Squares represent MP, triangles MHP, and rectangles MTFPP molecules, respectively. The dashed lines at 0 and 4.92 eV represent energy of H_2O and O_2, respectively. The gray area separates the metals from the group 9 and before from the 10 and after of the periodic table. The lines and equations are derived from the linear fit to the data points listed in Table 1.

MP.[4,8,9,34,37] It has been proposed that the 3D site of MHP could provide ways to break the scaling relations between *OH and *OOH; see for instance ref 8. This has been based on the assumption that the interaction of the hanging carboxylic group of the hangman scaffold with the *OH and *OOH reaction intermediates can stabilize/destabilize the intermediates to a different degree, and therefore break the scaling relation. However, our calculations show that the carboxylic group stabilizes both reaction intermediates in a similar way by formation of hydrogen bond between −COOH and OH/OOH. Moreover, our results reveal that the hangman scaffold possess a great flexibility in adapting its configuration to the local configuration of the reactive center, see Discussion below. Noteworthy is that the correlation between *O and *OH/ *OOH binding energies appears to be less correlated for the organometallic complexes studied here as compared metal and oxide surfaces.[9] The reason can be that the adsorption of O involves larger charge transfer (formally 2e) from the organometallic complex whereas the adsorption of OH/OOH requires less (formally 1e). In systems like metals and oxides, there is almost an infinite reservoir of electrons, and the *O can easily access required 2e. However, in the organometallic complex the number of electrons is limited, and electron transfer to the O makes much more pronounced changes to the electron structure than for the periodic metal/oxide structures. That stresses that fact that scaling relations are not obvious for molecular systems.

As reported in Table 1, binding energies of the *OH and *OOH decreases monotonically moving from left to right in the periodic table. This is attributed to the change in bond ionicity that decreases with increasing number of d-electrons in the valence shell of the metal. It is also observed that the position of *O changes for the different organometallic complexes. For the metals that bind intermediates stronger, the *O level is placed closer to *OH, whereas for the metals that bind intermediates weakly, the *O is positioned closer to

Table 1. Gibbs Free Energies in eV of the *OH, *O, and *OOH Adsorption for OER Intermediates Evaluated at $T = 300$ K[a]

	ΔG_{*OH}			ΔG_{*O}			ΔG_{*OOH}		
	MP	MTFPP	MHP	MP	MTFPP	MHP	MP	MTFPP	MHP
Cr	0.21	0.25	−0.04	−0.06	0.01	−0.08	3.26	3.48	2.80
Mn	0.54	0.40	0.31	0.79	0.89	1.26	3.28	3.34	3.39
Fe	0.66	0.71	0.50	1.47	1.59	1.46	3.64	3.67	3.57
Co	1.09	1.10	0.79	2.86	2.93	2.57	4.05	4.32	3.89
Ni	2.15	2.22	1.78	4.15	4.21	3.90	4.94	5.31	5.00
Cu	2.63	2.73	2.18	4.68	4.87	4.10	5.83	5.35	5.10
Ru	−0.52	−0.18	−0.15	0.15	0.26	0.37	2.31	2.81	2.59
Rh	0.69	0.56	0.58	2.61	3.01	2.38	3.58	3.64	3.63
Ag	2.56	2.85	1.57	4.66	4.83	3.96	5.00	5.13	4.82
Ir	0.63	0.68	0.46	2.13	2.15	1.97	3.62	3.88	3.52
Pt	2.50	2.54	2.16	4.51	4.59	3.91	5.37	5.65	4.49
Au	2.30	2.20	1.22	4.38	4.56	3.54	5.00	4.83	4.71
Zn	2.21	2.34	1.73	4.42	4.53	4.21	5.01	5.03	4.93
AD$_{MP}$		0.06	−0.36		0.13	−0.27		0.11	−0.17

[a]The last row contains an average deviation from ΔG of MPs (AD$_{MP}$) in eV and is calculated as a difference between the average values of $\Delta G_{MHP/MTFPP}^{OER}$ and ΔG_{MP}^{OER}.

the *OOH; see Figure 2 and Table 1. Thus, as the *OH and *OOH levels shift toward lower binding energy, the *O follow this trend but with different magnitude (see equations in Figure 2).

The metals that tend to bind adsorbates too strongly (the far left side of the plot) or too weakly (the far right side of the plot) correspond to two unfavorable extremes. In the former case the *OOH intermediate is not stable and likely to decompose into *OH and *O intermediates that will poison the electrode surface. This is true for metals like Cr. In the later extreme, for metals, e.g., Ni and Cu, the *OOH is too weakly bonded to the central metal atom (see Table 1), and there will not be any proton−electron transfer to the intermediate; thus, the reaction will not continue.[4]

The least thermodynamically favorable reaction step of all four electrochemical steps in OER/ORR defines the thermodynamical overpotential of the reaction for a given system. Analyzing activity (in our case the overpotential) as function of a descriptor (here *OH binding energy) results in a volcano shape relation as shown in Figure 3.

As shown in Figure 3, the apex of OER/ORR lies ~0.2 eV from the equilibrium electrode potential that defines maximum electrode efficiency from a thermodynamical standpoint. We find that in case of ORR, Co is unequivocally found to be the best catalytic metal for all of these three organometallic molecules; see Figure 3 and Table 2. This is in good agreement with experimental studies where Co has been suggested as the best catalytic metal.[21] For metals on the left side of the ORR volcano (group 9 and before of the periodic table), the reaction overpotential originates from the too strongly bonded *OH intermediates. That is, the potential losses in these systems will originate from additional potential needed to remove this reaction intermediate from the electrode, whereas on the right side (group 10 and after) the overpotential originates from too weakly bonded reaction intermediate. Moving to OER, we find that the most catalytically active metals for MP are Ir, Fe, and Co, for MTFPP are Ir and Fe, and for MHP are Co, Fe, Ir, and Rh; see Table 2 for details.

Close to the apex of the OER volcano, there is an intersection of the three lines that represent energy relations between the *OH−*O, *O−*OOH, and *OOH binding energies. Thus, using the *OH descriptor, the OER over-
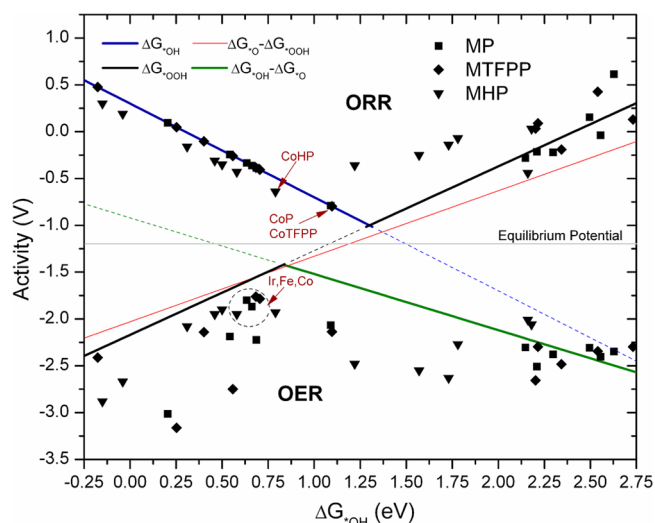
Figure 3. The activity trends plotted for MP, MTFPP, and MHP. ORR volcano is seen above and OER volcano below the equilibrium electrode potential. The points represent a calculated thermodynamical overpotential for each system as a function of *OH binding energy. The volcano lines have been derived from the scaling relation established in Figure 2. The gray line represents the equilibrium electrode potential at −1.23 V. For clarity, we have marked only the most active elements.

potential appears to be a more complicated function of the stability of reaction intermediates than the ORR overpotential. For example, we find that for Co and Ir the OER overpotential originates from the energy barrier between too strongly bonded *OH and *O, whereas for Fe it originates from the *O−*OOH energy barrier, for all three organometallic complexes investigated in this study. As shown in Figure 3, there is a well-behaved volcano relation for ORR. For OER, however, the volcano shape is not that distinct. This originates from the less pronounced correlation between *O and *OH/ *OOH as compared to *OH and *OOH intermediates. In case of OER, the catalytically significant steps involve the *O binding energies, and thus a less formed volcano shape appears. This suggests that for OER, a different descriptor could be more appropriate.

Table 2. Calculated $\eta^{0,OER}$ and $\eta^{0,ORR}$ in V for MP, MTFPP, and MHP

|	MP		MTFPP		MHP	
	OER	ORR	OER	ORR	OER	ORR
Cr	−1.79	1.33	−1.93	1.28	−1.44	1.42
Mn	−0.96	0.99	−0.91	1.13	−0.85	1.07
Fe	−0.64	0.87	−0.55	0.82	−0.67	0.88
Co	−0.84	0.44	−0.91	0.43	−0.70	0.59
Ni	−1.07	0.95	−1.07	1.32	−1.04	1.16
Cu	−1.12	1.84	−1.21	1.36	−0.83	1.26
Ru	−1.68	2.05	−1.18	1.71	−1.65	1.53
Rh	−1.00	0.84	−1.52	0.97	−0.72	0.80
Ag	−1.18	1.19	−1.32	1.23	−1.32	0.98
Ir	−0.57	0.90	−0.53	0.85	−0.72	0.92
Pt	−1.08	1.38	−1.12	1.66	−0.78	0.79
Au	−1.15	1.01	−1.43	1.26	−1.25	0.87
Zn	−1.28	1.01	−1.25	1.04	−1.40	1.09

As can be observed in Figure 3, even the metals with the lowest calculated thermodynamical overpotential are not at the apex of corresponding volcano plots, which suggest that there is room for improvements of their efficiency. This naturally led to the investigation of impact of the side groups and hangman scaffold on the reaction landscape as discussed in the following section.

Effect of the Side Groups and the Hangman Scaffold on the Reaction Landscapes. First we discuss the impact of the side groups by comparing the Gibbs free energies of the reaction intermediates between MPs and MTFPPs. According to our calculations (Table 1), addition of fluorophenyl side groups to the macrocycle results in an average shift toward lower binding energies of around 0.06, 0.13, and 0.11 eV for *OH, *O, and *OOH. In the literature, there are contradictory suggestions as to the effect of C_6F_5 groups on the charge reorganization in the organometallic complexes. For instance,

Linder et al. have suggested that charge reorganization is mostly related to the macrocycle, i.e., leaving the electronic structure of the central metal atom almost intact,[38] whereas in the work of Dogutan et al.[39] it is suggested that an addition of C_6F_5 groups can modify the oxidation state of the central metal atom, i.e., change from the formal Co(II) to Co(III) between CoP and CoTFPP/CoHP. In order to investigate any effect of the side groups on the electronic structure, we will compare CoP with CoTFPP. We calculated a decrease in ionization potential (IP) of 0.52 eV by addition of C_6F_5 to the CoP, which is consistent with the experimental decrease of ~0.6 eV.[38]

Figure 4 shows the one-electron Kohn−Sham levels together with a selection of the frontier orbitals for CoP and CoTFPP. Note that the energy levels correspond to both the spin-up and the spin-down channels.

The addition of C_6F_5 to CoP results in an energetic downshift of the electronic spectrum by 0.77 eV that is consistent with the calculated change in IP. The calculated HOMO−LUMO gap is virtually unchanged. Mulliken population analysis (MPA) reveals charges of +0.66/−1.64/+0.35 and +0.67/−1.65/+0.89 for the Co/N/C atoms of the CoP and CoTFPP (excluding C_6F_5 groups), respectively. This suggests that the electron-withdrawing C_6F_5 groups have marginal effect on the change of the oxidation state of the central metal atom, whereas their addition considerably changes the electron density of the carbon atoms. Thus, charge is drained from the C of CoP macrocycle upon addition of C_6F_5. More importantly, we do not find any significant changes in the occupation of the frontier molecular orbitals that could suggest that addition of the C_6F_5 could directly influence the oxidation state of the Co; see Figure 4. In both cases, the LUMO is localized on the cobalt and has pure d_{z^2} character. The HOMO and HOMO-1 of the CoP have clear macrocycle character and are preceded by the orbitals with $d_{xz/yz}$, d_{z^2}, and $d_{z^2−y^2}$ character. Despite a rearrangement of the positions between orbitals that are localized on the macrocycle (HOMO and HOMO-1 of the
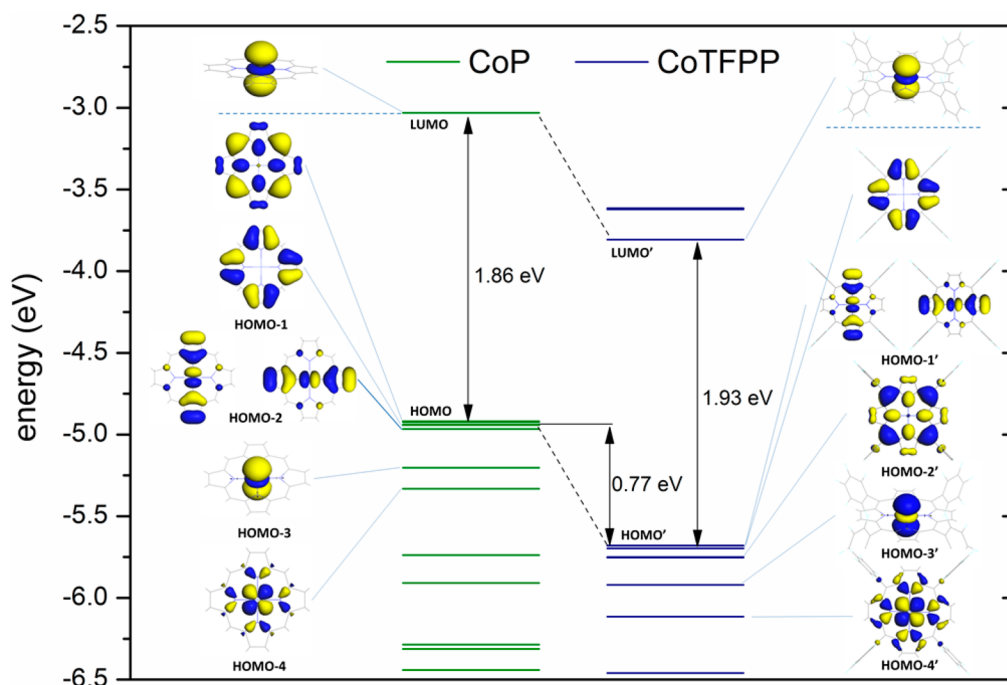
Figure 4. The discrete energy levels of the CoP (green) and CoTFPP (blue) as well as some their frontier orbitals.
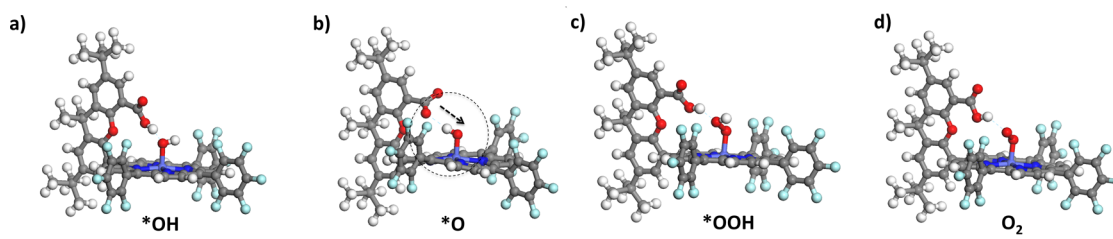
Figure 5. The ground state structures of the (a) *OH, (b) *O, (c) *OOH, and (d) O_2 intermediates for CoHP resulted from our calculations.

CoP), the occupancy of the Co-d localized orbitals of the CoTFPP as compared to CoP stays intact.

The calculations reveal that the hangman scaffold (including the carboxylic acid group) as well as the porphyrin macrocycle possesses considerable conformational flexibility. The entire xanthene scaffold is able to align either horizontally or vertically with respect to the macrocycle plane and even bend out of its molecular plane in order to maximize hydrogen−adsorbate bond as seen in Figure 5. In addition, the carboxylic acid group itself can rotate and align in overall to maximize the bond with the adsorbate. Also the macrocycle buckles or twists upon adsorption of the different reaction intermediate.

The slow reaction kinetics at the oxygen electrodes has been suggested to depend on the strength of the O−O bond.[10,40] Hence, an efficient catalytic material should facilitate the O−O bond dissociation.[41] In this context, the finding that the hangman scaffold only marginally changes the O−O (1.30 Å) and the OO−Co (1.90 Å) as compared to CoP of 1.30 and 1.91 Å, is rather surprising. The assumption has previously been that the O−O bond is further activated (elongated) when the hangman carboxylic group is introduced to, for example, CoP.[40] Our calculated MPA yields that the charge on the Co atom changes from +0.66/+0.68 to +0.79/+0.81 as O_2 is adsorbed for CoP and CoHP, respectively. This is accompanied by a charging of the O_2 molecule by 0.3e. Moreover, adsorption of O_2 onto CoP/CoHP quenches the net spin (one unpaired electron) on the cobalt site of the bare CoP/CoHP. Such changes in charge and spin density can be interpreted as transfer of one electron from the metal atom to the $2\pi^*$ antibonding orbital of O_2, which results in a change of the formal oxidation state of the Co from II to III and the formation of a superoxo complex $[Co^{3+}O_2^{\bullet-}]$. We find that the O_2 bond activation is virtually the same for CoP and CoHP, which is in full agreement with the mechanism proposed for O_2 activation by various metallo-oxygenases.[11]

Our calculations reveal that addition of the hangman scaffold to the macrocycle stabilizes adsorption of *OH, *O, and *OOH by −0.36, −0.27, and −0.17 eV, respectively, as compared to MPs; see Table 1. This rather even stabilization of all three reaction intermediates by the hangman scaffold originates mostly from the formation of a hydrogen bond between the carboxylic acid group and the adsorbate (see Figure 5). Interestingly, we find that in case of the CoHP the proton is transferred to *O without any barrier and that the energy gain is as large as −0.53 eV. This result in stabilization of the otherwise too weakly bonded *O intermediate. Although the calculated thermodynamical overpotential does not indicate higher activity of CoHP over CoP as found experimentally,[39] our calculations indicate a possible explanation for its higher performance. That is, addition of the hangman motif to the macrocycle does not break universal relation between *OH and *OOH; however because of the mobile proton of the

carboxylic group, the *O intermediate can be placed in more favorable position between these two levels, thereby resulting in a higher activity. It should be noted that the values of the calculated overpotential are sensitive to the input energies of the reaction intermediates. There are several reasons why there is a discrepancy between the calculated and the experimental activity for these systems, including the approximation to the XC-functional and solvation effects, and especially the nature of local structure of water molecules around the active center appears to be important. In the experiments, these complexes are deposited on an electrode material that may influence the catalytic activity of these systems.

In summary, the suggested higher activity observed for the MHPs as correspond to MPs from a thermodynamical standpoint can be explained by a concerted action of the electron-withdrawing side groups, which destabilize all reaction intermediates, and the hangman motif, which selectivity stabilizes the oxygen intermediate. In fact, our calculations reveal that replacing the carboxylic acid group (−COOH) of the hangman scaffold with acidity constant pK_a of 4.76 by sulfonic group (−SO_3H) with much lower pK_a of −2.81[42] results in further stabilization of the *O. We find −0.51 and −0.78 eV stabilization of the *O level for the Co and Ni, respectively, for the hangman with a sulfonic acid group over the one with a carboxylic acid group. The calculated OER/ORR overpotentials for Co- and Ni-hangman complexes with sulfonic acid group are of 0.67/0.79 and 0.68/0.88 V, respectively. Therefore, replacing the carboxylic by sulfonic group brings only small changes in the OER/ORR over-potential of CoHP, where the O* level is already in good position (2.57 as compared to 2.46 eV of an ideal catalyst). However the sulfonic group decreases significantly the overpotential of NiHP of 1.04/1.16 V, where *O level is significantly underbinded (3.90 eV); see Table 1. It should be noted that both acid groups are most likely fully dissociated in the solvent medium but serve here as an example of a possible pathway to affect the OER/ORR landscape. To summarize, our results demonstrate that by careful selection of the side groups of porphyrin macrocycle and proton-donating group of the hangman (e.g., with different acidity constant), it is possible to tune the adsorption energy of the reaction intermediates toward better performance of these molecular catalytic materials.

■ CONCLUSIONS

This work provides one more step toward understanding and developing low cost catalysts based on the organometallic complexes for OER/ORR. We have identified the most catalytically active central metal atoms for MPs, MTFPPs, and MHPs studied here. Furthermore, linear scaling relation between the adsorption energy of *OH and *OOH is valid also for organometallic complexes, and the addition of 3D scaffold

to the macrocycle ring does not break this relation. The addition of electron-withdrawing groups to a porphyrine macrocycle destabilizes the adsorption energy of the all reaction intermediates. By transferring proton from its acid group to the *O intermediate, the hangman scaffold can shift this level into more favorable energetic position. To conclude, our calculations suggest that there may be possible further improvement of these catalytic materials by careful selection of side group of the macrocycle and acid groups of the hangman scaffold.

■ ASSOCIATED CONTENT

Ⓢ Supporting Information

Calculated selected bond distances and angles of the ground state CoH compared with crystallographic data; table with a number of the unpaired electrons in the reaction intermediates; table of the total energies of the reaction intermediates in Ha; coordinates. This information is available free of charge via the Internet at http://pubs.acs.org.

■ AUTHOR INFORMATION

Corresponding Author
jakub.baran@chalmers.se; anders.hellman@chalmers.se
Notes
The authors declare no competing financial interest.

■ ACKNOWLEDGMENTS

■ REFERENCES

(1) Markovic, N. M. P. N. R.; Ross, P. N. CATTECH 2000, 4, 110.
(2) Symes, M. D.; Cronin, L. Nat. Chem. 2013, 5, 403.
(3) Ford, D. C.; Nilekar, A. U.; Xu, Y.; Mavrikakis, M. Surf. Sci. 2010, 604, 1565.
(4) Norskov, J. K.; Rossmeisl, J.; Logadottir, A.; Lindqvist, L.; Kitchin, J. R.; Bligaard, T.; Jonsson, H. J. Phys. Chem. B 2004, 108, 17886.
(5) Rossmeisl, J.; Dimitrievski, K.; Siegbahn, P.; Norskov, J. K. J. Phys. Chem. C 2007, 111, 18821.
(6) Trasatti, S. Electrochim. Acta 1991, 36, 225.
(7) Beer, H. B. J. Electrochem. Soc. 1980, 127, 303C.
(8) Calle-Vallejo, F.; Martinez, J. I.; Rossmeisl, J. Phys. Chem. Chem. Phys. 2011, 13, 15639.
(9) Man, I. C.; Su, H. Y.; Calle-Vallejo, F.; Hansen, H. A.; Martinez, J. I.; Inoglu, N. G.; Kitchin, J.; Jaramillo, T. F.; Norskov, J. K.; Rossmeisl, J. ChemCatChem 2011, 3, 1159.
(10) Shook, R. L.; Borovik, A. S. Inorg. Chem. 2010, 49, 3646.
(11) Que, L.; Tolman, W. B. Nature 2008, 455, 333.
(12) Deng, C. Z.; Dignam, M. J. J. Electrochem. Soc. 1998, 145, 3507.
(13) Jasinski, R. J. Electrochem. Soc. 1965, 112, 526.
(14) Choi, A.; Jeong, H.; Kim, S.; Jo, S.; Jeon, S. Electrochim. Acta 2008, 53, 2579.
(15) Sun, S.; Jiang, N.; Xia, D. J. Phys. Chem. C 2011, 115, 9511.
(16) He, H.; Lei, Y.; Xiao, C.; Chu, D.; Chen, R.; Wang, G. J. Phys. Chem. C 2012, 116, 16038.
(17) Carver, C. T.; Matson, B. D.; Mayer, J. M. J. Am. Chem. Soc. 2012, 134, 5444.
(18) Peljo, P.; Murtomäi, L.; Kallio, T.; Xu, H.-J.; Meyer, M.; Gros, C. P.; Barbe, J.-M.; Girault, H. H.; Laasonen, K.; Kontturi, K. J. Am. Chem. Soc. 2012, 134, 5974.
(19) Fukuzumi, S.; Mandal, S.; Mase, K.; Ohkubo, K.; Park, H.; Benet-Buchholz, J.; Nam, W.; Llobet, A. J. Am. Chem. Soc. 2012, 134, 9906.
(20) Dogutan, D. K.; Bediako, D. K.; Teets, T. S.; Schwalbe, M.; Nocera, D. G. Org. Lett. 2010, 12, 1036.
(21) McGuire, R., Jr.; Dogutan, D. K.; Teets, T. S.; Suntivich, J.; Shao-Horn, Y.; Nocera, D. G. Chem. Sci. 2010, 1, 411.
(22) Rosenthal, J.; Nocera, D. G. In Progress in Inorganic Chemistry; John Wiley & Sons, Inc.: New York, 2008, p 483.
(23) Dogutan, D. K.; Stoian, S. A.; McGuire, R.; Schwalbe, M.; Teets, T. S.; Nocera, D. G. J. Am. Chem. Soc. 2010, 133, 131.
(24) Chang, C. J.; Chng, L. L.; Nocera, D. G. J. Am. Chem. Soc. 2003, 125, 1866.
(25) Delley, B. J. Chem. Phys. 1990, 92, 508.
(26) Delley, B. J. Chem. Phys. 2000, 113, 7756.
(27) Delley, B. Int. J. Quantum Chem. 1998, 69, 423.
(28) Lee, C.; Yang, W.; Parr, R. G. Phys. Rev. B 1988, 37, 785.
(29) Broyden, C. G. IMA J. Appl. Math. 1970, 6, 76.
(30) Marom, N.; Kronik, L. Appl. Phys. A: Mater. Sci. Process. 2009, 95, 159.
(31) Cramer, C. J.; Truhlar, D. G. Phys. Chem. Chem. Phys. 2009, 11, 10757.
(32) Walker, F. A.; Lo, M.-W.; Ree, M. T. J. Am. Chem. Soc. 1976, 98, 5552.
(33) Greeley, J.; Jaramillo, T. F.; Bonde, J.; Chorkendorff, I. B.; Norskov, J. K. Nat. Mater. 2006, 5, 909.
(34) Rossmeisl, J.; Qu, Z. W.; Zhu, H.; Kroes, G. J.; Norskov, J. K. J. Electroanal. Chem. 2007, 607, 83.
(35) Kurth, S.; Perdew, J. P.; Blaha, P. Int. J. Quantum Chem. 1999, 75, 889.
(36) Lide, D. R. CRC Handbook of Chemistry and Physics, 90th ed.; CRC Press/ Taylor and Francis: Boca Raton, FL, 2010; CD-ROM version.
(37) Calle-Vallejo, F.; Martinez, J. I.; Garcia-Lastra, J. M.; Abad, E.; Koper, M. T. M. Surf. Sci. 2013, 607, 47.
(38) Lindner, S.; Treske, U.; Grobosch, M.; Knupfer, M. Appl. Phys. A: Mater. Sci. Process. 2011, 105, 921.
(39) Dogutan, D. K.; McGuire, R.; Nocera, D. G. J. Am. Chem. Soc. 2011, 133, 9178.
(40) Lai, W.; Cao, R.; Dong, G.; Shaik, S.; Yao, J.; Chen, H. J. Phys. Chem. Lett. 2012, 3, 2315.
(41) Orellana, W. J. Phys. Chem. C 2013, 117, 9812.
(42) Guthrie, J. P. Can. J. Chem. 1978, 56, 2342.